Engineering Science and Technology, an International Journal 48 (2023) 101559

Contents lists available at ScienceDirect

Engineering Science and Technology, an International Journal

journal homepage: www.elsevier.com/locate/jestch

Full length article

Analysis of PV power plant performance considering combination of different MPPT algorithms, shading patterns and connection types☆

Cagri Batuhan Oguz [a], Emre Avci [a], Salih Baris Ozturk [b,*]

[a] Department of Electrical and Electronics Engineering, Duzce University, 81620, Duzce, Türkiye
[b] Department of Electrical Engineering, Istanbul Technical University, 34469 Maslak, Istanbul, Türkiye

ARTICLE INFO

Keywords:
Maximum power point tracking (MPPT)
Partial shading pattern
Photovoltaic (PV)
PV power plant
Connection type
Solar energy
Partial shading condition (PSC)

ABSTRACT

The effeteness of MPPT algorithms is deteriorated by having more Maximum Power Points (MPPs) on the characteristics of the PV array. The number of MPPs can increase with the different connection types of PV panels and the pattern of partial shading, and it also changes the P–V (Power–Voltage) characteristics of the panel. Therefore, it is important to consider different combinations of algorithms, connection types and partial shading patterns for an effective PV plant design. This study assesses the performance of a PV power plant including a 5 × 5 PV array by considering eight different connection types, six partial shading conditions (PSCs), and three well-known MPPT algorithms, all together, on the TMS320F28335 DSP platform. The obtained results and analyses show that the TCT (Total Cross Tied) connection type has higher performance than the other connection types under all PSCs with an average of 25.98% Mismatched Loss (ML), 54.3% Fill Factor (FF) and 13.45% efficiency (η). As for the shading patterns, the Diagonal (DG) pattern has less effect on the system's ML and FF values, and the Long Wide (LW) pattern is less effective in reducing system η. Regarding the algorithms, it has been proven that the performance of a PV system using the simplest form of the basic algorithms can reach the performance of the system using complex algorithms when the connection type is well-adjusted according to the shading patterns. Overall, the given analyses and results prove the significance of taking into account the combination of different MPPT algorithms, types of panel connections, and partial shading patterns to enhance PV system power efficiency and reduce the complexity of PV power plant installations.

1. Introduction

As the global population grows and energy consumption rises, the deficit in fossil fuels is becoming more prominent, revealing the significance of using renewable energy sources (RESs) [1,2]. The growth of fields and applications that utilize solar energy, which is a widely preferred type among RES, has played an important role in reducing the dependency on fossil fuels in the electrical power generation policies of countries [3]. Photovoltaic (PV) panels that allow solar energy harvesting contribute to reducing environmental concerns. Moreover, easy installation, lower maintenance cost, and non-dynamic structures make the PV systems feasible for individual users and large-scale renewable energy-based electrical power generation systems [4,5].

Due to these factors, the effectiveness of PV systems' energy conversion has taken center stage. Nevertheless, the effectiveness of PV systems is significantly impacted by environmental conditions like temperature and insolation. It also depends on the PV panel's intrinsic nonlinear properties (I–V, or current–voltage, and P–V, or power–voltage) [6]. Engineers and scientists in this industry are thus interested in getting the most power possible from PV panels. Therefore, achieving high efficiency in PV systems requires an MPPT approach. By adjusting the power converters that are being used, such as the DC–DC converter and inverter, the PV panel is compelled to operate at the highest voltage and current points in this method.

In the last decade, several MPPT algorithms have been developed and implemented with many contributions to ensure that the PV panel's electrical power will be at its peak value under different conditions. Many of these maximum power extraction schemes can be assessed with their performance criteria, such as accuracy, dynamic behavior, and complexity [7,8]. However, it is commonly preferred to categorize MPPT algorithms as conventional, intelligent, optimization, and hybrid methods [9–11]. For conventional MPPT algorithms, the Constant Voltage (CV), Open Circuit Voltage (OCV), Incremental Conductance (InC)

☆ Peer review under responsibility of Karabuk University.

* Corresponding author.
E-mail addresses: cagri43960@ogr.duzce.edu.tr (C.B. Oguz), emreavci@duzce.edu.tr (E. Avci), ozturksb@itu.edu.tr (S.B. Ozturk).

https://doi.org/10.1016/j.jestch.2023.101559
Received 24 May 2023; Received in revised form 4 October 2023; Accepted 22 October 2023
Available online 16 November 2023

Nomenclature

ΔI_L	Converter inductance current ripple
ΔP	Change in PV array power for P&O algorithm
ΔV	Change in PV array voltage for P&O algorithm
ΔV_{out}	Converter output voltage ripple
η	Efficiency of a PV system
A	Quality factor of PV panel
B	Boltzmann constant
c_1	Cognitive learning coefficient
c_2	Social learning coefficient
C_{in}	Input capacitor of the converter
C_{out}	Output capacitor of the converter
D	Diode in PV panel model
d	Duty cycle
dD	Duty perturbation
dP	Change in PV array power for InC algorithm
dV	Change in PV array input for InC algorithm
dV	Change in PV array voltage for InC algorithm
f_{sw}	Switching frequency
G_{best}	Global best particle
I_c	Panel output current in a column
I_D	Diode saturation current in PV panel model
I_{in}	Converter input current
I_k	PV array output current for each step
I_{out}	Converter output current
I_{ph}	Generated current by PV panel
$I_{PV,MPP}$	PV array current at maximum power point
I_{PV}	Panel output current
I_r	Panel output current in a row
I_{SC}	Short circuit current of PV panel
k	Iteration number
L	Converter inductance
N_p	Number of parallel connected panel
N_s	Number of series connected panel
P_{best}	Best particle
P_k	PV array instantaneous power for each step
P_{MPP}	Power at the maximum power point
q	Elementary charges
r_1	Random value between 0 and 1
r_2	Random value between 0 and 1
R_p	Equivalent parallel resistor in PV panel model
R_s	Equivalent series resistor in PV panel model
T	Temperature in Kelvin
v_i^k	Current velocity vector
V_c	Panel output voltage in a column
V_{in-max}	Maximum converter input voltage
V_{in}	Converter input voltage
V_k	PV array output voltage for each step
V_{OC}	Open circuit voltage of PV panel
$V_{out-max}$	Maximum converter output voltage
V_{out}	Converter output voltage
$V_{PV,MPP}$	PV array voltage at maximum power point
V_{PV}	Panel output voltage
V_r	Panel output voltage in a row
x_i	ith particle position
ACO	Ant Colony Optimization
ANN	Artificial Neural Network
BL	Bridge Link
BL-HC	Bridge Link-Honey Comb
BL-TCT	Bridge Link-Total Cross Tied
CS	Cuckoo Search
CV	Constant Voltage
DG	Diagonal
DSP	Digital Signal Processor
FF	Fill Factor
FLC	Fuzzy Logic Controller
GM	Global Maximum
GMP	Global Maximum Power
GMP(P)	GMP value under PSC
GMP(S)	GMP value under standard test conditions
GWO	Grey Wolf Optimization
HC	Honey Comb
HC-TCT	Honey Comb-Total Cross Tied
IL	Irradiance Level
InC	Incremental Conductance
LM	Local Maximum
LMP	Local Maximum Power
LN	Long Narrow
LW	Long Wide
ML	Mismatched Loss
MPP	Maximum Power Point
MPPT	Maximum Power Point Tracking
NI	Number of iteration
NP	Number of particles
OCV	Open Circuit Voltage
P&O	Perturbation and Observe
PIL	Processor-In-The-Loop
PSC	Partial Shading Condition
PSO	Particle Swarm Optimization
PWM	Pulse Width Modulation
RES	Renewable Energy Source
SN	Short Narrow
SP	Series Parallel
SP-TCT	Series Parallel-Total Cross Tied
SW	Short Wide
TCT	Total Cross Tied
US	Unshaded
w	Inertia weight

and Perturbation and Observe (P&O) algorithms, which are commonly known algorithms, form the basis of MPPT techniques [12]. With the advantages of a fast dynamic response, simple structure, and lower computational burden, these conventional algorithms mostly perform superior Maximum Power Point (MPP) tracking capability at stable and uniform external conditions. However, once the Partial Shading Condition (PSC) occurs, where the PV panels are exposed to different levels of irradiance, the characteristics of the PV array are recast from monotonic to non-monotonic one. Under this condition, the unsatisfactory performance of the conventional algorithms initiates a quest to find an improved version.

Additionally, apart from the conventional algorithms, intelligent and optimization algorithms are adopted for the MPPT system, which

can be found in the literature as Fuzzy Logic Controller (FLC), Artificial Neural Network (ANN), Cuckoo Search (CS), Ant Colony Optimization (ACO), Particle Swarm Optimization (PSO), and Grey Wolf Optimization (GWO) algorithms and many more. As with conventional algorithms, these algorithms have enhanced variants that improve the system performance under PSC [13–20]. Furthermore, not only does PSC affect the performance of these algorithms, but also, the connection type of the PV panels affects the performance of all the MPPT algorithms, where P–V characteristics have multiple peak points known as Local Maximum (LM) as in PSC. Therefore, it is understood that the connection types of PV panels and PSC make it difficult to capture the Global Maximum (GM) point on the P–V curve of the PV arrays for all MPPT algorithms, especially when different partial shading patterns are examined together with different PV panel connections.

Most recently, improved versions of the aforementioned algorithms, mainly focused on the PSO, P&O and InC, can be found in this field to overcome having multiple MPPs. In [21,22], a hybrid and in [23,24], modified P&O methods are suggested to improve the effectiveness of the MPPT algorithm in a variety of environmental circumstances. An FLC-based algorithm is developed in [25] to improve MPPT efficiency. In [26], a self-adapted InC algorithm with high dynamic and steady-state performance is given for different operating points on the P–V characteristics. A modified InC algorithm stated in [27] eliminates some drawbacks of conventional InC. In [28–31], the enhanced PSO algorithms are given to improve their accuracy under PSC.

In the references given so far, the PSCs are only exemplified in a few cases, and also the proposed algorithms are not tested under changing panel connection types. On the other hand, the following studies present more comprehensive cases in terms of the algorithm, connection type and PSC. For instance, In [32], 132 PV panels are used with different partial shading patterns to test the enhanced PSO algorithm. In [33], the PSCs are formed with 4 partial shadings patterns and for 3 different PV panels to test the optimal PSO parameters. In [34], a fully adaptive PSO algorithm is developed and tested under the PSC that includes 10 × 5 PV panels and only one connection type in simulation and 3 PV panels for experimental studies. In [35], an analysis of the proposed PSO algorithm under PSC is given for a few PV array characteristics. With a new connection method named magic square, [36] uses 5 × 5 PV panels and 6 shading patterns in simulation studies to compare the proposed connection method without assessing any algorithm. Similarly, [37] analyzes the effectiveness of the different connection types in various PSCs using simulation results. As seen above literature review, the studies mainly focus on either improving an MPPT algorithm or connection type. This situation has caused the problem of which MPPT algorithm should be used together with which connection type, according to the partial shading patterns that the power plant will be exposed to during the installation of PV power plants. In the literature, a study to analyze the effectiveness of a PV plant by considering the combination of MPPT algorithms, partial shading patterns and connection types has yet to be found.

Inspired by the above discussions, in this study, for a 5 × 5 PV array using 6 different shading conditions and 8 different connection types together, the basic forms of three mostly preferred algorithms P&O, InC and PSO are executed in Processor-In-The-Loop (PIL) platform. Moreover, the impact of the connection types on the efficiency of the MPPT system considered with different partial shading patterns according to the Fill Factor (*FF*), Mismatched Loss (*ML*), and Efficiency (η) performance criteria is also analyzed. The key advancements outlined in this paper can be succinctly summarized as follows; (1) the conventional MPPT algorithms can achieve a high success rate in reaching MPP by selecting the appropriate panel connection type according to the shading pattern to be exposed, (2) the DG shading pattern may not pose a severe problem for the power efficiency of the PV system, (3) under the LW and DG shading pattern, the algorithm and connection type to be selected for the PV system has almost no effect on the system performance. As a result, the proposed system reveals the importance of considering the MPPT algorithm, connection types and partial shading patterns altogether for the power efficiency and complexity of PV power plants to be installed.

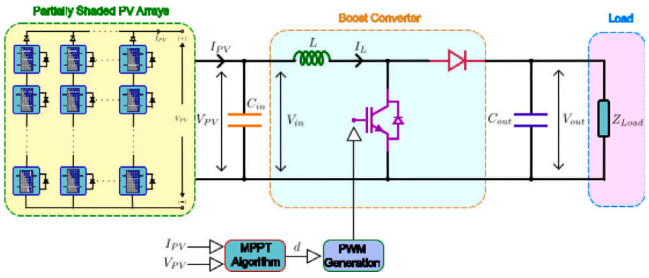

Fig. 1. The designed MPPT system.

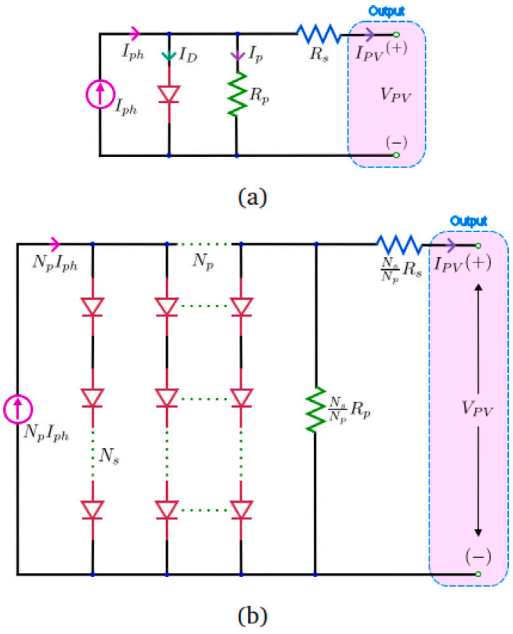

Fig. 2. Single diode circuit model of (a) PV panel (b) $N_s \times N_p$ PV array.

The rest of this paper is organized as follows; An MPPT system structure and modeling are given in Section 2. The principles of the three algorithms and details are provided in Section 3. Section 4 introduces the eight connection types and five shading patterns with their P–V characteristics, *FF*, *ML*, and efficiency (η) criteria. In Section 5, the designed 5 × 5 PV array with the different algorithms is tested according to the shading patterns and connection types. The results obtained by the PIL system and remarks on the study are also listed in this section. Finally, the conclusion of this work is briefly given in Section 6.

2. System description and modeling

In a PV system, the power produced by the array is transferred to the load unit, grid, or other equipment using a power converter to set the voltage and current at the PV array's output to the appropriate level. To stabilize the load voltage, a DC–DC converter, which is one of the most popular power converters used in MPPT systems, is placed in between the PV array and the load. The output voltage of the PV array is boosted in this study to form an MPPT system using a DC–DC boost-type converter. Fig. 1 provides the general block diagram of the designed MPPT system. As seen in Fig. 1, the C_{in} capacitor is located near the PV array's output to smooth the PV output voltage.

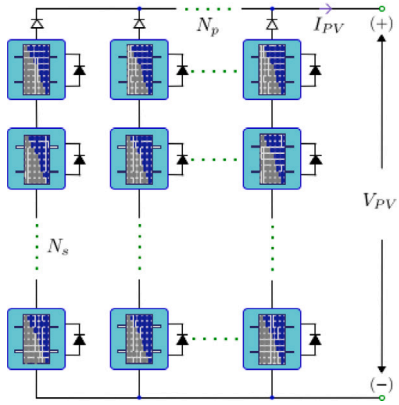

Fig. 3. Configuration of the $N_s \times N_p$ PV array under PSC.

Table 1
Parameters of the designed DC–DC boost type converter.

Parameter	Value
Rated Power	5.375 kW
Output voltage (V_{out}) and its ripple (ΔV_{out})	400 V - 1%
Inductance current ripple (ΔI_L)	5%
Switching frequency (f_{sw})	5 kHz

With the aid of a MOSFET semiconductor switch, a diode, and the converter's inductance (L), the DC–DC converter converts this voltage. Then, the converter output voltage is filtered with a C_{out} capacitor. Given in Eq. (1) is the relationship between the converter's output and input, where d is the duty ratio of the switching signals and V_{out}, I_{out}, V_{in}, and I_{in} are the converter's output voltage and current, converter's input voltage and current, respectively. The value of the L inductance is determined as 8.78 mH with the help of Eq. (2) using the parameters mentioned in Table 1 (but 8.8 mH is used). The C_{out} capacitor is calculated as 448 μF (but 450 μF is selected) with Eq. (3), where ΔI_L is the inductance current ripple, ΔV_{out} is the ripple voltage at the output, f_{sw} is the switching frequency, $V_{in,max}$ and $V_{out,max}$ are the minimum and maximum values of the converter input and output voltages, respectively.

$$\frac{V_{out}}{V_{in}} = \frac{I_{in}}{I_{out}} = \frac{1}{1-d} \tag{1}$$

$$L = \frac{V_{in,max}(V_{out,max} - V_{in,max})}{V_{out,max}\Delta I_L f_{sw}} \tag{2}$$

$$C = \frac{I_{out,max}(V_{out,max} - V_{in,max})}{V_{out,max}\Delta V_{out} f_{sw}} \tag{3}$$

The MPPT algorithm calculates the duty ratio using the sensed PV array output voltage and current, as shown in Fig. 1. The power produced by the PV array should be transferred to the load at the converter output using the maximum power of the calculated d. To do this, the PV array impedance at the maximum power point should match the load value. Using Eq. (1), the relationship between the impedance of the load and the PV array is given in Eq. (4), where $I_{PV,MPP}$ and $V_{PV,MPP}$ are the current and voltage of the PV array at the MPP, respectively. According to this equation and the PV panel characteristics (which will be given later), the impedance at the load is calculated as 40 Ω.

$$Z_{load} = \frac{1}{(1-d)^2}\frac{V_{PV,MPP}}{I_{PV,MPP}} \tag{4}$$

For a PV-MPPT system, the I–V and P–V characteristics of the PV panel are essential to perceive the MPPs of the system. These characteristics are obtained with the modeling of the PV panel. In the literature, the circuit model of a PV panel can be found with the single [38], double [39], or three diodes [40] model. In Fig. 2, the circuit diagram of a panel and $N_s \times N_p$ PV array are given with a single-diode model. Using Kirchhoff's current and voltage law in the figure, the output current (I_{PV}) of the panel can be calculated as in Eq. (5), where V_{PV} is the panel output voltage, I_{ph} is the generated current by the panel, I_D is the diode (D) saturation current, A is the diode quality factor, q is the elementary charges equals to 1.6e−19 C, T is the temperature in Kelvin, B is the Boltzmann constant equals to 1.3865e−23 J/K, R_s and R_p are the equivalent series and shunt resistances, respectively. In this work, the Kyocera KD215GX PV solar panel is employed for all studies, and its electrical parameters can be found in Table 2, where I_{SC} is the short circuit current, V_{OC} is the open circuit voltage, V_{MPP}, I_{MPP}, and P_{MPP} are the panel voltage, current and output power at the MPP, respectively. In many PV systems, the number of series connected (N_s) and the number of parallel connected (N_p) PV panels are used, as in Fig. 3, to increase the power or output voltage of the PV array. The model can be reconfigured in this case as in Eq. (6).

Table 2
The specifications of the Kyocera solar KD215GX PV panel.

Parameter	Value
Open circuit voltage, V_{OC}	33.2 V
Short circuit current, I_{SC}	8.78 A
The voltage at the maximum power point, V_{MPP}	26.6 V
Current at the maximum power point, I_{MPP}	8.09 A
Maximum power, P_{MPP}	215.2 W
Temperature coefficient of V_{OC}	−0.33
Temperature coefficient of I_{SC}	0.02
Dimensions (in cm)	150.01 × 99.01

When a PSC occurs in $N_s \times N_p$ PV array, the shaded module generates a current less than the ones without shades; therefore, the shaded panel output voltage would be negative where the shaded panel behaves as if it is a load. This results in a decreased system efficiency and hotspot effect on the panel, which may damage it. To solve this issue, the PV panels are connected in parallel with a bypass diode under partial shading conditions (PSCs), as shown in Fig. 3. As a result, in the characteristics of the PV array, multiple MPPs occur, making it difficult to detect global ones in the MPPT algorithm.

$$I_{PV} = I_{ph} - I_D\left[exp(\frac{V_{PV} + R_s I_{PV}}{ABT}q) - 1\right] - \frac{V_{PV} + R_s I_{PV}}{R_p} \tag{5}$$

$$I_{PV} = N_p I_{ph} - I_D N_p\left[exp(\frac{V_{PV}N_p + N_s R_s I_{PV}}{ABTN_s R_p}q) - 1\right] - \frac{V_{PV}N_p + R_s I_{PV}N_s}{R_p N_s} \tag{6}$$

3. Principles of the MPPT algorithms

The employed algorithm in the MPPT system has an essential role in the PV system efficiency. Especially under different PCSs and connection types, its performance may differ. Therefore, in this study, the three most widely preferred MPPT algorithms are put in perspective, as mentioned in Section 1. Being one of them, the P&O algorithm perturbs the operating voltage of the PV array and observes the output power until reaching the MPP of the array. The algorithm uses the measured PV array output voltage (V_k) and current (I_k) to calculate the instantaneous power (P_k) for each time step (k). The change in the power (ΔP) is calculated by comparing instantaneous power with the previous power value ($P_k - 1$). And also, the change in the voltage (ΔV) is calculated with its previous value ($V_k - 1$). And then, as shown in Fig. 4(a), this algorithm checks the sign of the ΔP. If the ΔP is a positive value, the voltage perturbation is continued with the previous direction according to the sign of the ΔV by adding a positive or negative small duty perturbation ($d\,D$). If the ΔP is negative, the instantaneous

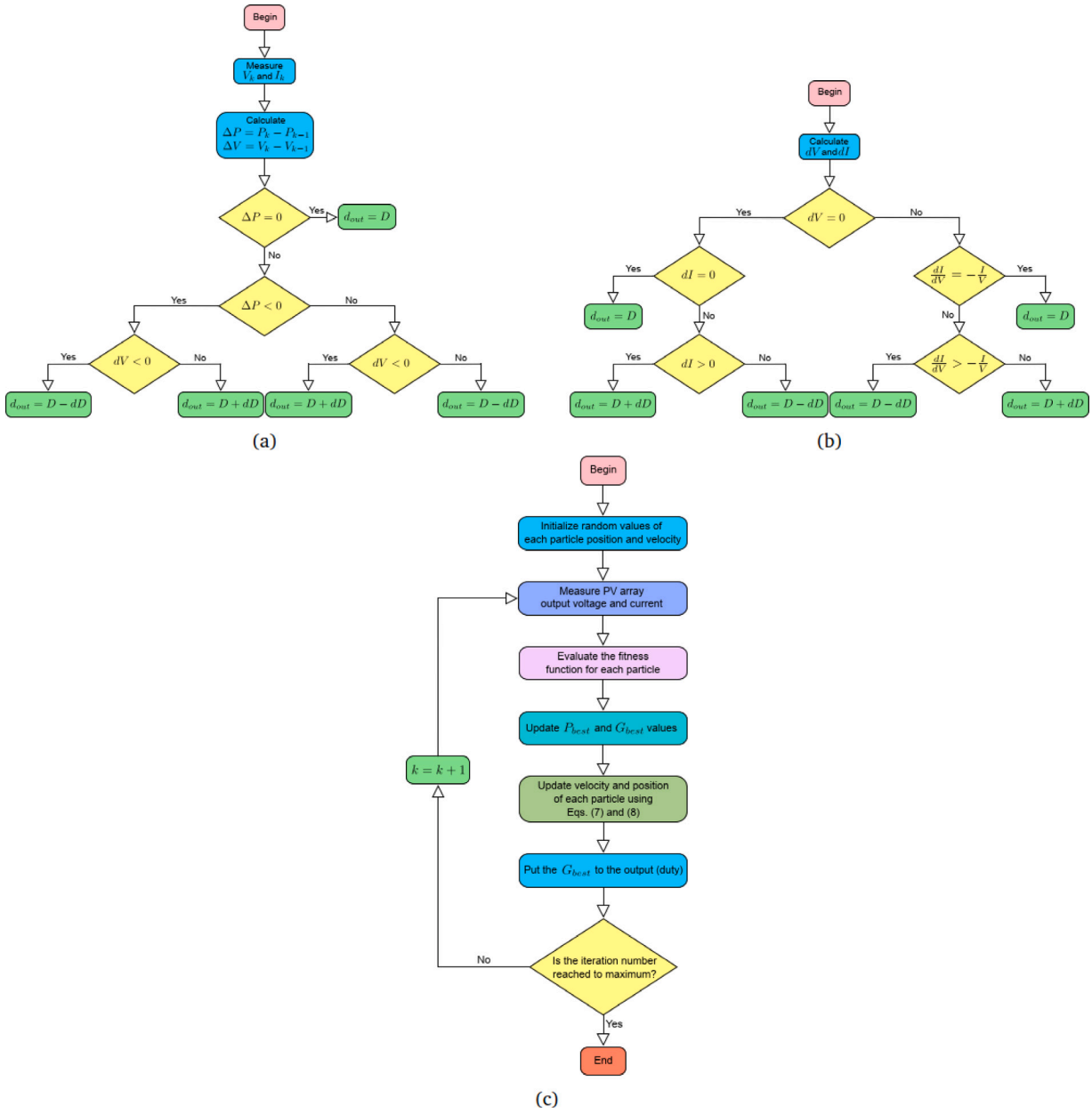

Fig. 4. Flow chart of the basic (a) P&O algorithm (b) InC algorithm (c) PSO algorithm.

power is not at the MPP of the array characteristics, and the voltage perturbation direction is reversed.

As in the P&O algorithm, the InC algorithm uses the PV array output voltage and current measurements to calculate the change in the voltage (dV) and current (dI) using the previous values of these parameters. The algorithm works by adjusting the slope of the P–V characteristics of the array to be zero ($dP/dV = 0$) at the MPP. Therefore, the sum of the instantaneous conductance (I/V) and the incremental conductance (dI/dV) should be equal to zero ($(dI/dV) + (I/V) = 0$) at the MPP. When the condition (dI/dV) $>$ ($-I/V$) is satisfied, the duty value should be decreased with a small duty perturbation (dD). Oppositely, in the condition (dI/dV) $<$ ($-I/V$), the duty is increased by adding the dD. When dV and dI values are equal to zero, the operating power reaches the MPP. The flowchart of the detailed algorithm is shown in Fig. 4(b).

Unlike the aforementioned two algorithms, the PSO algorithm is an intelligent optimization technique based on the foraging of the birds in a flock. In this algorithm, each particle in a swarm typifies a candidate solution. Their position (x_i) is adjusted according to the best particle (P_{best}) in a neighboring and the global best particle (G_{best}) in all populations by aping the success of themselves. In a search space, the position of the particles is updated in each iteration (k) using Eq. (7),

$$x_i^{k+1} = x_i^k + v_i^{k+1} \tag{7}$$

where v_i^{k+1} component represents the next velocity vector and is calculated as follows;

$$v_i^{k+1} = wv_i^k + r_1c_1[P_{best} - x_i^k] + r_2c_2[G_{best} - x_i^k] \tag{8}$$

where w is the inertia weight, v_i^k is the current velocity vector, c_1 and c_2 are the cognitive and social learning coefficients, respectively, r_1 and r_2 are random values in the $(0-1)$ range and i is the number of particles (NP). This velocity definition can be found with many different variants, as given in [41], which focus mainly on the divergence problem of the particles. The other parameters in Eq. (8) that affect the algorithm performance are c_1 and c_2, also referred to as trust parameters. With $c_1 > 0$ and $c_2 = 0$, all particles pretend to be

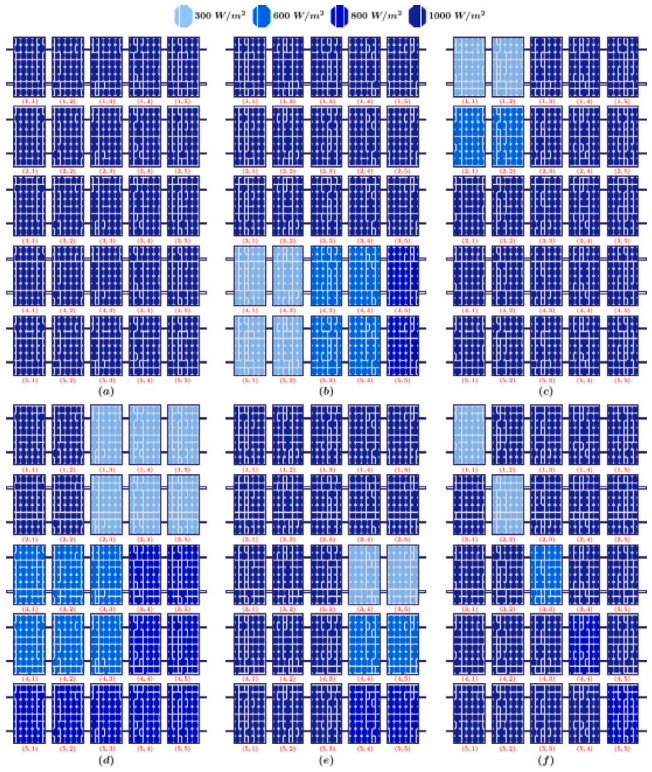

Fig. 5. 5 × 5 PV array shading patterns (a) Unshaded (US) ($P_{d,max}$ = 5385 W) (b) Short Wide (SW) ($P_{d,max}$ = 4347.04 W) (c) Short Narrow (SN) ($P_{d,max}$ = 4906.56 W) (d) Long Wide (LW) ($P_{d,max}$ = 3572.32 W) (e) Long Narrow (LN) ($P_{d,max}$ = 4820.48 W) (f) Diagonal (DG) ($P_{d,max}$ = 4906.56 W).

independent local searchers. When $c_2 > 0$ and $c_1 = 0$, all particles are converged to a single point. In many applications, the condition $c_1 = c_2$ is used, which causes particles to converge towards the average of P_{best} and G_{best}. However, the correlation between c_1 and c_2 depends on the applications. Therefore, there should be a good balance between these parameters [42,43]. In the literature, many ways to determine the PSO parameters can be found, which are population size, number of iterations (NI), trust parameters, inertia weight, etc. They have different effectiveness and performance under the selected PV panel connection type and the partial shading pattern in the MPPT system. In this study, a basic form of the PSO algorithm is employed, illustrated in the flow chart shown in Fig. 4(c). The parameters for this algorithm are set as $c_1 = c_2 = 2$, $w = 0.2$, $NP = 3$, and $NI = 300$. The flow charts given in Fig. 4 constitute the conventional type of algorithm, while many advanced and optimized versions that are not within the scope of this study can be found in the literature. Consequently, the results of this study will guide the reader to search or enhance the algorithm selected for the particular connection type and partial shading pattern in a PV system.

4. Configuration of PV array

In an MPPT approach used in the PV system, the ability of the system to detect and converge MPP should be tested under different partial shading patterns and connection types because the efficiency of the system differs not only with the employed MPPT algorithm but also with partial shading patterns and connection types. Therefore, six partial shading patterns and eight connection types, which are mostly considered in a PV system, will be considered in this section.

4.1. Partial shading patterns

In a PV system, the PSC can seriously decrease the overall system power depending on the shading pattern that will occur. Therefore, the partial shading problem should be evaluated with many different patterns that can simulate the real environmental condition of the PV array. For this purpose, six different patterns, which are the Unshaded (US), Short Narrow (SN), Short Wide (SW), Long Wide (LW), Long Narrow (LN), and Diagonal (DG) patterns, are considered in the PV system that has 25 identical PV panels (parameters can be seen in Table 2) in this work. These panels are in a matrix form with 5 rows and 5 columns. It means 5 panels are used in a row, and the system has 5 columns. The location of a panel is stated as (i, k), where i represents the row number, and k represents the column number. When all panels are considered discrete, there is no connection; the total PV system power can be calculated using Eq. (9), where IL is the irradiance value of the corresponding PV panel.

$$P_{d,max} = \sum_{k=1}^{5}\sum_{i=1}^{5} \frac{IL}{1000} P_{MPP}(i,k) \tag{9}$$

In the US pattern, all the PV panels expose the same irradiation with 1000 W/m^2 as in Fig. 5(a), where the $P_{d,max}$ value of the array is 5385 W. In the SW pattern, the (4, 1), (4, 2), (5, 1), and (5, 2) panels have 300 W/m^2 irradiation, (4, 3), (4, 4), (5, 3) and (5, 4) panels have 600 W/m^2 irradiation, the (4, 5) and (5, 5) panels have 800 W/m^2 irradiation, and the rest of the panels expose 1000 W/m^2 irradiation as in Fig. 5(b), where the $P_{d,max}$ value of the array is 4347.04 W. In the SN pattern, (1, 1) and (1, 2) panels have 300 W/m^2 irradiation, (2, 1) and (2, 2) panels have 600 W/m^2 irradiation, and the others have 1000 W/m^2 irradiation as in Fig. 5(c), where the $P_{d,max}$ value of the array is 4906.56 W. In the LW pattern, six panels have 300 W/m^2 irradiation, the other six panels have 600 W/m^2 irradiation, nine panels have 800 W/m^2 irradiation, and the rest of the panels expose 1000 W/m^2 irradiation, as given in Fig. 5(d). In this shading pattern the $P_{d,max}$ value of the array is 3572.32 W. In the LN pattern, the (3,4) and (3,5) panels have 300 W/m^2 irradiation, (4,4) and (4,5) panels have 600 W/m^2 irradiation, the panels (5,4) and (5,5) have 800 W/m^2 irradiation, and the rest of the panels expose 1000 W/m^2 irradiation as in Fig. 5(e), where the $P_{d,max}$ value of the array is 4820.48 W. In the DG pattern, only the diagonally located panels are shaded, as seen in Fig. 5(f). In this shading pattern, the $P_{d,max}$ value of the array is 4906.56 W. With the given $P_{d,max}$ values, it is clear that the partial shading pattern causes the different $P_{d,max}$ values. However, the output power of the array may significantly deviate from the $P_{d,max}$ value according to its connection type.

4.2. Connection types

In the PV array installation process, the panel connection type is generally decided according to the required PV array output voltage and power, with the most known options: series and parallel connections. However, with this approach, the assessment of the efficiency of the whole system under different PSCs and/or with different MPPT algorithms is omitted. Therefore, the most known PV array connection types, which are given in Fig. 6 as the Series Parallel (SP), Bridge Link (BL), Honey Comb-Total Cross Tied (HC-TCT), Bridge Link-Total Cross Tied (BL-TCT), Series Parallel-Total Cross Tied (SP-TCT), Honey Comb (HC), Total Cross Tied (TCT), and Bridge Link-Honey Comb (BL-HC) will be examined in this section. Four of the connection types can be considered the basic connection types, while the others can be considered as their hybrid variants.

With a simple structure and easy-to-implement advantages, the widely used connection type SP is formed by connecting a series of all panels in a column with each other and connecting parallel each column as in Fig. 6(a). The high number of panels connected in series makes the SP connection perform poorly, especially under PSCs. In this

Table 3
Local Maximum Power (LMP) and Global Maximum Power (GMP) of different connection types (in watts) under different PSCs.

	US	SW	SN	LW	LN	DG
SP	5346 W (GMP)	3051 W (LMP) 3130 W (GMP)	3325 W (LMP-1) 3902 W (LMP-2) 4111 W (GMP)	1787 W (LMP-1) 2483 W (LMP-2) 2494 W (GMP)	3217 W (LMP-1) 3912 W (LMP-2) 4176 W (GMP)	3336 W (LMP) **4238 W (GMP)**
TCT	5346 W (GMP)	3110 W (LMP) 3130 W (GMP)	3130 W (LMP-1) 3849 W (LMP-2) 4279 W (GMP)	2215 W (LMP) 3323 W (GMP)	3006 W (LMP-1) 3813 W (LMP-2) 4264 W (GMP)	2957 W (LMP) **4790 W (GMP)**
BL	5346 W (GMP)	3081 W (LMP) 3130 W (GMP)	3187 W (LMP-1) 3989 W (LMP-2) 4064 W (GMP)	2440 W (LMP) 2809 W (GMP)	3192 W (LMP-1) 3942 W (LMP-2) 3995 W (GMP)	2986 W (LMP) **4751 W (GMP)**
HC	5346 W (GMP)	3076 W (LMP) 3130 W (GMP)	3217 W (LMP-1) 4008 W (LMP-2) 4011 W (GMP)	2441 W (LMP-1) 2481 W (LMP-2) 2786 W (GMP)	3155 W (LMP-1) 3960 W (LMP-2) 4031 W (GMP)	3043 W (LMP-1) 3907 W (LMP-2) **4472 W (GMP)**
SP-TCT	5346 W (GMP)	3090 W (LMP) 3130 W (GMP)	3130 W (LMP-1) 3849 W (LMP-2) **4189 W (GMP)**	2215 W (LMP) 3324 W (GMP)	3006 W (LMP-1) 3912 W (LMP-2) 4176 W (GMP)	3228 W (LMP-1) 3972 W (LMP-2) 4155 W (GMP)
BL-TCT	5346 W (GMP)	3092 W (LMP) 3130 W (GMP)	3130 W (LMP-1) 3948 W (LMP-2) 4188 W (GMP)	2216 W (LMP) 3324 W (GMP)	3006 W (LMP-1) 3872 W (LMP-2) 4202 W (GMP)	2943 W (LMP) **4787 W (GMP)**
BL-HC	5346 W (GMP)	3110 W (LMP) 3130 W (GMP)	3167 W (LMP-1) 3974 W (LMP-2) 4112 W (GMP)	1651 W (LMP-1) 2325 W (LMP-2) 2654 W (LMP-3) 2862 W (GMP)	3110 W (LMP-1) 3930 W (LMP-2) 4071 W (GMP)	3035 W (LMP) **4761 W (GMP)**
HC-TCT	5346 W(GMP)	3098 W (LMP) 3130 W (GMP)	3130 W (LMP-1) 3948 W (LMP-2) 4198 W (GMP)	2216 W (LMP) 3324 W (GMP)	3006 W (LMP-1) 3912 W (LMP-2) 4176 W (GMP)	2011 W (LMP) **4765 W (GMP)**

Table 4
ML, *FF* and η values of the array for different connection types under different partial shading patterns.

SP Connection				**TCT Connection**				**BL Connection**				**HC Connection**			
	ML(%)	**FF(%)**	**η(%)**		**ML(%)**	**FF(%)**	**η(%)**		**ML(%)**	**FF(%)**	**η(%)**		**ML(%)**	**FF(%)**	**η(%)**
SW	41.45	42.95	10.43	**SW**	41.45	42.95	10.43	**SW**	41.45	42.95	10.43	**SW**	41.45	42.95	10.43
SN	23.10	56.41	12.14	**SN**	19.96	58.71	12.63	**SN**	23.98	55.76	12.00	**SN**	24.97	55.04	11.85
LW	53.35	34.22	**12.92**	**LW**	37.84	45.59	**17.21**	**LW**	47.46	38.54	**14.55**	**LW**	47.89	38.23	**14.43**
LN	21.89	57.30	12.55	**LN**	20.24	58.51	12.82	**LN**	25.27	54.82	12.01	**LN**	24.60	55.31	12.12
DG	**20.73**	**58.15**	12.52	**DG**	**10.40**	**65.73**	14.15	**DG**	**11.13**	**65.19**	13.21	**DG**	**16.35**	**61.36**	12.27
SP-TCT Connection				**BL-TCT Connection**				**BL-HC Connection**				**HC-TCT Connection**			
	ML(%)	**FF(%)**	**η(%)**		**ML(%)**	**FF(%)**	**η(%)**		**ML(%)**	**FF(%)**	**η(%)**		**ML(%)**	**FF(%)**	**η(%)**
SW	41.45	42.95	10.43	**SW**	41.45	42.95	10.43	**SW**	41.45	42.95	10.43	**SW**	41.45	42.95	10.43
SN	**21.64**	**57.47**	12.37	**SN**	21.66	57.47	12.37	**SN**	23.08	56.42	12.14	**SN**	21.47	57.60	12.40
LW	37.82	45.61	**17.22**	**LW**	37.83	45.61	**17.22**	**LW**	46.46	39.27	**14.83**	**LW**	37.82	45.61	**17.22**
LN	21.89	57.30	12.55	**LN**	21.40	57.66	12.63	**LN**	23.85	55.86	12.24	**LN**	21.88	57.30	12.55
DG	22.28	57.01	14.14	**DG**	**10.45**	**65.68**	14.06	**DG**	**10.94**	**65.33**	14.06	**DG**	**10.87**	**65.38**	14.07

connection type, the array output voltage is equal to the total voltage of each panel in a column, and the sum of the currents in each row gives the array output current. Therefore, with uniform *IL* conditions in the SP connection, the output voltage and current are equal to the total voltage of the panels in a column and the total current of the panels in a row [44,45]. The array power ($P_{a,r}$) can be calculated as $25V_cI_r$ using Eq. (10), where V_c is the panel output voltage in a column, and I_r is the output current of a panel in a row.

$$P_{a,r} = \left[\sum_{k=1}^{5} V(i,k)\right]_{i=[1,5]} \times \left[\sum_{i=1}^{5} I(i,k)\right]_{k=[1,5]} \tag{10}$$

In the TCT connection, all panels in a row are connected in parallel with each other in that row, and a row is connected in series with the next row. This cross-connection, as in Fig. 6(b), increases the complexity, wiring cost, and cable losses. However, this type of connection performs better under PSCs than under SP [44,45]. The array power ($P_{a,c}$) can be calculated as $25V_rI_c$ using Eq. (11), where V_r is the output voltage of a panel in a row and I_c is the output current of a panel in a column.

The BL connection type is derived from the TCT and SP types overcoming the disadvantage of requiring more wiring. Unfavorably, it has low performance under PSCs because of reduced array output voltage. This connection type is obtained by forming four panels as a bridge rectifier unit, where two of the four PV panels are connected in series, and the attained two groups are connected in parallel with each other. Then, all the bridges are crossly connected, as shown in Fig. 6(c). This type of connection includes more series connections as opposed to TCT and fewer compared to SP; therefore, the performance of PSC is better than SP and worse than TCT [44,45]. Under uniform *IL* conditions, the array output power of this type can be calculated as $25V_cI_r$ using Eq. (10).

The HC connection type inspires the hexagonal structure of the honey bee house. As shown in Fig. 6(d), this type includes more series connections as opposed to BL and TCT and fewer compared to SP; therefore, the PSC performance of it is better than SP and worse than BL and TCT [44,45]. Under uniform *IL* conditions, the array output power of this type can be calculated as $25V_cI_r$ using Eq. (10).

$$P_{a,c} = \left[\sum_{i=1}^{5} V(i,k)\right]_{k=[1,5]} \times \left[\sum_{k=1}^{5} I(i,k)\right]_{i=[1,5]} \tag{11}$$

The rest of the connection types given in Fig. 6(e), (f), (g) and (h) are the hybrid connection types developed by combining the first four. The array output power of these hybrid types under uniform *IL* conditions can be calculated as $25V_cI_r$ using Eq. (10).

As for the efficiency under PSCs, these connection types have very different characteristics because the current paths in every row and every column will differ according to the partial shading pattern. In Fig. 7, the P–V characteristics of all connection types under the six patterns are given, where the 25 PV panels are identical, and their parameters can be seen in Table 2. The value of Global Maximum Power

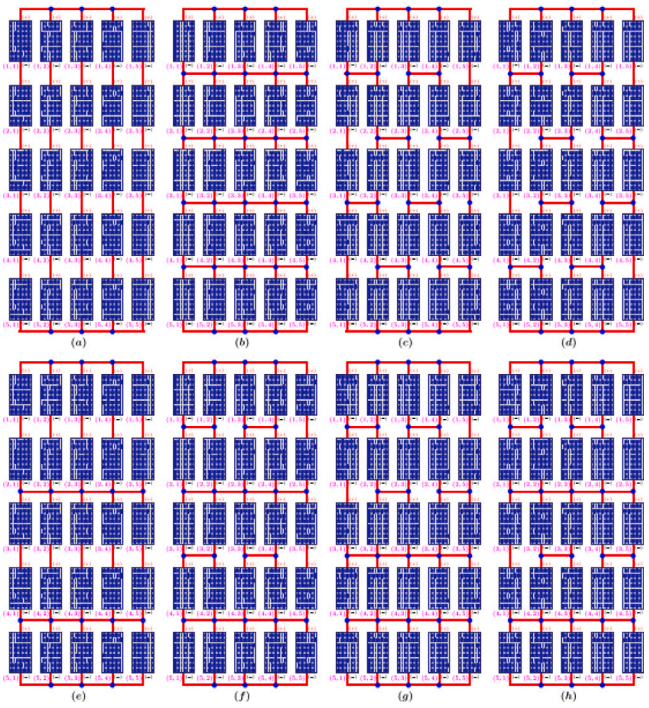

Fig. 6. 5 × 5 PV array connection types (a) SP ($P_{a,r} = 25V_cI_r$) (b) TCT ($P_{a,c} = 25V_rI_c$) (c) BL ($P_{a,r} = 25V_cI_r$) (d) HC ($P_{a,r} = 25V_cI_r$) (e) SP-TCT ($P_{a,r} = 25V_cI_r$) (f) BL-TCT ($P_{a,r} = 25V_cI_r$) (g) BL-HC ($P_{a,r} = 25V_cI_r$) (h) HC-TCT ($P_{a,r} = 25V_cI_r$).

(GMP) and Local Maximum Power (LMP) of these characteristics are given in Table 3, where the red colored power indicates the maximum output power of each connection type. As shown in Fig. 7 and Table 3, the SP connection type has 5346 W output power when there is no PSC (US pattern), however; with the changing shading pattern, the P–V characteristics of the SP have two or three MPPs. Among the shading patterns, the SP connection type reaches 4238 W maximum output power under the DG pattern. In the characteristics of this connection under the LW shading pattern, the fact that the LMP-2 and GMP points are very close to each other (11 W difference) will make it difficult for MPPT algorithms to catch the GMP. In the TCT connection type, the array output power has 4790 W maximum output power under the DG pattern. Also, under the SW pattern, the LMP and GMP points are very close to each other in the TCT connection type with a 20 W difference. The same situation can be seen in the HC connection under the SN pattern with only a 3 W difference and the BL-HC connection under the SW pattern with a 20 W difference. BL, HC, BL-TCT, BL-HC, and HC-TCT connection types also reach their maximum output power with 4751 W, 4472 W, 4787 W, 4761 W, and 4765 W under the DG pattern, respectively. Differing from these connection types, only the SP-TCT connection type has its maximum output power under the SN pattern. The output power of the SP-TCT type under SN, LN and DG conditions are very close to each other.

Apart from the P–V characteristics curves, the performance of the connection types is also assessed with the calculation of the Fill Factor (FF), Mismatch Power Loss (ML) and Efficiency (η). The ML of an array in any connection type indicates the power differences between standard test conditions and PSC. It is calculated as in Eq. (12), where $GMP(S)$ is the GMP value under standard test conditions, and $GMP(P)$ is the GMP value under PSC. Another criterion for the effectiveness is the Fill Factor that can be calculated as in Eq. (13), where V_{OC} and I_{SC} are the open circuit voltage and short circuit current, respectively. The higher value of the FF indicates a higher performance of the array. The last criterion is the efficiency that can be formulated as in Eq. (14), where A is the area of the array. These three criteria for the given eight connection types and six partial shading patterns are calculated as in Table 4 using Eq. (12), Eq. (13), Eq. (14) and Table 3. In Table 4, the minimum ML of each connection type among the shading patterns are given with blue color. Similarly, the maximum FF and η of each connection type among the shading patterns are given in red and green colors, respectively.

$$ML(\%) = \frac{GMP(S) - GMP(P)}{GMP(S)} \times 100 \tag{12}$$

$$FF(\%) = \frac{GMP(P)}{V_{OC} \times I_{SC}} \times 100 \tag{13}$$

$$\eta(\%) = \frac{GMP(P)}{IL \times A} \times 100 \tag{14}$$

5. PIL results and performance evaluation

To assess the effectiveness of the three distinct MPPT algorithms and connection types under a variety of partial shading circumstances, the proposed MPPT-based PV power plant system is developed utilizing the PIL (Processor-In-The-Loop) platform. In the PIL-based MPPT system, unlike a regular simulation, the power stage is simulated in the software, whereas the algorithm is verified digitally in the hardware target microprocessor. Therefore, the algorithm in the PIL implementation can be tested in a real-time DSP with the C/C++ language.

In this work, to create six different PV array shading patterns in PSIM® software, 25 Kyocera solar KD215GX PV panels are exposed to corresponding irradiation levels, given in Fig. 5, for each connection type shown in Fig. 6. At the output of the PV array, the designed DC–DC boost converter is employed to boost the PV array voltage level to the appropriate level for the load. In this way, the power stage of the system for different shading patterns and connection types is created in the software. On the other hand, the three MPPT algorithms are executed by the TMS320F28335 DSP evaluation board. As seen in Fig. 8, the DSP receives the PV array voltage and current measurements via JTAG communication and the USB cable connected between the PC and the DSP kit. Then, the MPPT algorithm calculates the duty ratio and is sent back to the simulated converter. In this way, to demonstrate the performance of the P&O, InC, and PSO algorithms outlined in Section 3, as well as the effectiveness of the connection types, these algorithms are executed by the TMS320F28335 DSP evaluation board for all eight connection types under six different shading patterns.

In Table 5, the PIL-based results are given, which categorize the measured output power of the system as the local or global maximum in accordance with the GMPs and LMPs data given in Table 3. As can be seen there, the PSO algorithm achieves finding the global maximum point of 45 out of 48 P–V characteristics, which means it has a success rate of 93.75%. It sticks to the local maximum power of the HC and SP connections under the SN shading pattern and of the SP connection under the LW shading pattern. These fails of the PSO arise from the fact that the GMP and LMP of the HC connection type under the SN pattern and of the SP connection type under the LW pattern are very close to each other (the difference is only 7 W and 11 W, respectively). Conversely, this success rate is around 33.33% and 31.25% for the InC and P&O algorithms, respectively. They fail with all connection types under the SW shading pattern to reach the global maximum point. Under this shading pattern, the maximum loss due to the conventional algorithms occurs in SP connection with 79 W, as shown in Table 5, whose numerical values are given in Table 3. This loss has a peak value of 959 W under the LN shading pattern with the SP connection. The detailed findings and remarks are listed below.

- The connection types and shading patterns greatly influence the maximum output power of the PV system.
- The TCT connection has the highest output power among the eight connection types, with 4790 W.

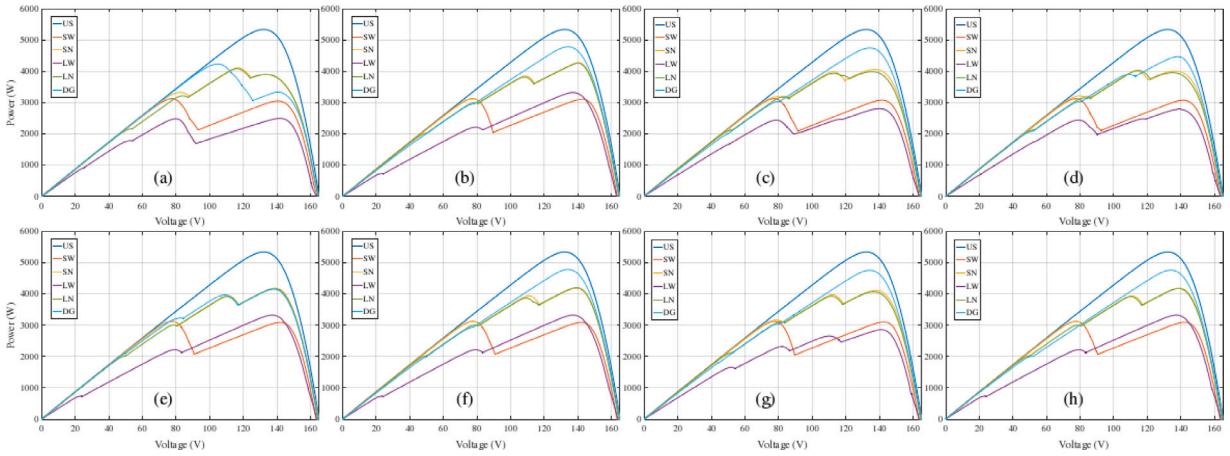

Fig. 7. P–V characteristics of (a) SP (b) TCT (c) BL (d) HC (e) SP-TCT (f) BL-TCT (g) BL-HC (h) HC-TCT connection types under eight different partial shading patterns.

Table 5
PIL-based output results of the 5 × 5 PV system for different algorithms, shading patterns, and connection types.

Shading Pattern: US				Shading Pattern: SN				Shading Pattern: SW			
Type of Connection	**PSO**	**InC**	**P&O**	**Type of Connection**	**PSO**	**InC**	**P&O**	**Type of Connection**	**PSO**	**InC**	**P&O**
BL	GMP	GMP	GMP	BL	GMP	LMP-2	GMP	BL	GMP	LMP	LMP
BL-HC	GMP	GMP	GMP	BL-HC	GMP	GMP	GMP	BL-HC	GMP	LMP	LMP
BL-TCT	GMP	GMP	GMP	BL-TCT	GMP	GMP	GMP	BL-TCT	GMP	LMP	LMP
HC	GMP	GMP	GMP	HC	LMP-2	LMP-2	LMP-2	HC	GMP	LMP	LMP
HC-TCT	GMP	GMP	GMP	HC-TCT	GMP	GMP	GMP	HC-TCT	GMP	LMP	LMP
SP	GMP	GMP	GMP	SP	LMP-2	LMP-2	LMP-2	SP	GMP	LMP	LMP
SP-TCT	GMP	GMP	GMP	SP-TCT	GMP	GMP	GMP	SP-TCT	GMP	LMP	LMP
TCT	GMP	GMP	GMP	TCT	GMP	GMP	GMP	TCT	GMP	LMP	LMP
Shading Pattern: LN				**Shading Pattern: LW**				**Shading Pattern: DG**			
Type of Connection	**PSO**	**InC**	**P&O**	**Type of Connection**	**PSO**	**InC**	**P&O**	**Type of Connection**	**PSO**	**InC**	**P&O**
BL	GMP	GMP	GMP	BL	GMP	GMP	GMP	BL	GMP	GMP	GMP
BL-HC	GMP	LMP-2	LMP-2	BL-HC	GMP	GMP	GMP	BL-HC	GMP	GMP	GMP
BL-TCT	GMP	GMP	GMP	BL-TCT	GMP	GMP	GMP	BL-TCT	GMP	GMP	GMP
HC	GMP	LMP-2	LMP-2	HC	GMP	GMP	GMP	HC	GMP	GMP	GMP
HC-TCT	GMP	GMP	GMP	HC-TCT	GMP	GMP	GMP	HC-TCT	GMP	GMP	GMP
SP	GMP	LMP-1	LMP-1	SP	LMP-2	LMP-2	LMP-2	SP	GMP	LMP	LMP
SP-TCT	GMP	GMP	GMP	SP-TCT	GMP	GMP	GMP	SP-TCT	GMP	GMP	GMP
TCT	GMP	GMP	GMP	TCT	GMP	GMP	GMP	TCT	GMP	GMP	GMP

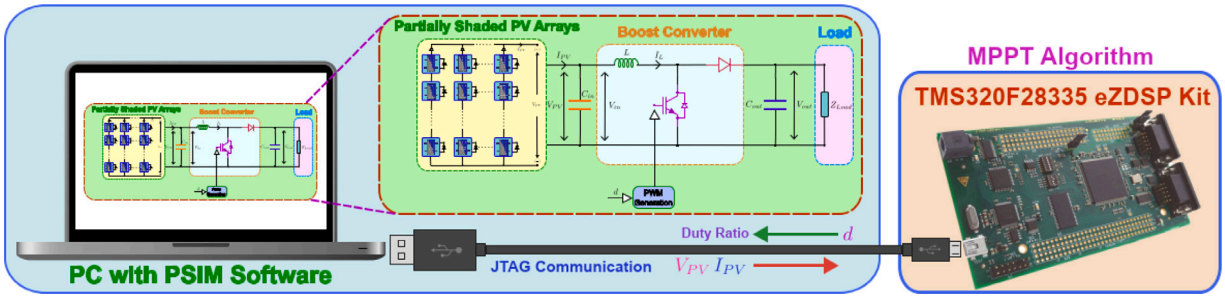

Fig. 8. Processor-In-The-Loop (PIL) implementation of the MPPT system.

- Among the five shading patterns, all connection types have maximum power under the DG pattern (excluding the SP-TCT connection). Also, all connection types have their minimum ML under this pattern (excluding SP-TCT connection). Correlatively, the FF of all connection types (excluding SP-TCT connection) reaches their maximum under the DG pattern. Therefore, the DG shading pattern may not pose a severe problem for the power efficiency of the system. However, the efficiency (η) of all connection types has the highest value under the LW pattern.
- If the connection type of a PV system is selected according to the shading pattern, the performance of the system using the simplest form of conventional algorithms can perform as high as the system using a complex one. For instance, under the SN shading pattern, if one of the BL-HC, BL-TCT, TCT, and SP-TCT connection types is employed, the performance of the system will be the same for the conventional and complex algorithms. Similarly, using one of the BL, BL-TCT, HC-TCT, TCT, and SP-TCT connection types will result in the same situation under the LN pattern.
- For the PV system, the employed MPPT algorithm significantly affects the reaching point in the P–V characteristics of the PV array for various connection types and shading patterns. Therefore, to test the performance of an MPPT algorithm, not only the different connection types or shading patterns but also both should be used together.

- Among the tested algorithms, the PSO reaches the GMP of the P–V characteristics under almost all tested shading patterns and connection types. However, it fails in the HC connection under the SN shading pattern and in the SP connection under the LW shading pattern because their global and local maximum points are very close. Therefore, if a PSO algorithm is employed and it is required to reach the GMPs under all shading patterns and connection types, an enhanced/improved or hybrid version of the algorithm should be developed or adapted.
- Though the conventional algorithms reach fewer global points than the PSO in all given conditions, they have almost the same performance as PSO under the LW and DG patterns with all connection types. Therefore, if the shading patterns are predicted to be LW and DG, the employed algorithm and the type of connection will not make a difference. In this case, the lowest-cost connection type and the lowest-complexity algorithm can be used.
- Under the SW shading pattern, it is crucial to use the PSO algorithm, as the global maximum point cannot be reached by conventional methods with all connection types. Additionally, if an algorithm that can reach the GMP is employed, the type of connection will not make a difference because the GMP of all connections has the same value under this pattern.

6. Conclusion

This paper has detailly analyzed the performance of a PV power plant consisting of a 5 × 5 PV array according to the MPPT algorithm, connection type, and shading pattern with the TMS320F28335 DSP kit-based Processor-In-The-Loop (PIL) platform. The effectiveness of the SP, TCT, HC, BL, SP-TCT, BL-TCT, BL-HC, and HC-TCT connection types are investigated with the parameters ML, FF and efficiency (η) under different shading patterns. With these criteria, the TCT-type connection exhibits better performance than the others under the SN, SW, LN, LW, and DG shading patterns. It reaches its peak output power under the diagonal (DG) shading patterns. Also, it has a maximum Fill Factor (FF) of 65.73% and a minimum Mismatch Power Loss (ML) of 10.40%. The used connection types and shading patterns make it possible to widely evaluate the performance of the employed PSO, P&O, and InC algorithms. The results of the algorithms show that the PSO algorithm has superior performance as expected among the other algorithms to reach the global maximum point of the P–V curve under different connection types and shading patterns. However, in 3 of 48 test cases, the PSO algorithm fails, which means that the enhanced version of it should be employed when a 100% success rate is expected. On the other hand, in 35 of 48 cases, the three algorithms perform similarly; therefore, a complicated MPPT algorithm may not be required in the majority of the shading patterns by choosing an appropriate connection type. Additionally, the proposed system can be used to assess the performance of any MPPT algorithm and also be used to decide the algorithm and connection type of any PV power plant to be installed.

Declaration of competing interest

The authors declare that they have no known competing financial interests or personal relationships that could have appeared to influence the work reported in this paper.

References

[1] N. Sockeel, J. Gafford, B. Papari, M. Mazzola, Virtual inertia emulator-based model predictive control for grid frequency regulation considering high penetration of inverter-based energy storage system, IEEE Trans. Sustain. Energy 11 (2020) 2932–2939, http://dx.doi.org/10.1109/TSTE.2020.2982348.

[2] Z. Shi, W. Wang, Y. Huang, P. Li, L. Dong, Simultaneous optimization of renewable energy and energy storage capacity with the hierarchical control, CSEE J. Power Energy Syst. 8 (2022) 95–104, http://dx.doi.org/10.17775/CSEEJPES.2019.01470.

[3] A. Cinco-Solis, J.J. Camacho-Escoto, L. Orozco-Barbosa, J. Gomez, PPAASS: Practical power-aware duty cycle algorithm for solar energy harvesting sensors, IEEE Access 10 (2022) 117855–117870, http://dx.doi.org/10.1109/ACCESS.2022.3220695.

[4] M.S. Chowdhury, K.S. Rahman, T. Chowdhury, N. Nuthammachot, K. Techato, M. Akhtaruzzaman, S.K. Tiong, K. Sopian, N. Amin, An overview of solar photovoltaic panels' end-of-life material recycling, Energy Strategy Rev. 27 (2020) 100431, http://dx.doi.org/10.1016/j.esr.2019.100431.

[5] S.K. Nag, T.K. Gangopadhyay, J. Paserba, Solar photovoltaics: A brief history of technologies [History], IEEE Power Electron. Mag. 20 (2022) 77–85, http://dx.doi.org/10.1109/mpe.2022.3150814.

[6] B. Yang, J. Wang, X. Zhang, T. Yu, W. Yao, H. Shu, F. Zeng, L. Sun, Comprehensive overview of meta-heuristic algorithm applications on PV cell parameter identification, Energy Conv. Manag. 208 (2020) 112595, http://dx.doi.org/10.1016/j.enconman.2020.112595.

[7] S. Motahhir, A. El Hammoumi, A. El Ghzizal, The most used MPPT algorithms: Review and the suitable low-cost embedded board for each algorithm, J. Clean. Prod. 246 (2020) 118983, http://dx.doi.org/10.1016/j.jclepro.2019.118983.

[8] D. Xu, H. Chen, X. Wang, V. Pires, J. Martins, A. Anuchin, X. Li, R. Palka, J. Gu, Coupling analysis of differential power processing-based PV system and its decoupling implementation of synchronous MPPT control, 70, 2023, pp. 6973–6983, http://dx.doi.org/10.1109/TIE.2022.3201277,

[9] M. Sarvi, A. Azadian, A comprehensive review and classified comparison of MPPT algorithms in PV systems, Energy Syst. 13 (2022) 281–320, http://dx.doi.org/10.1007/s12667-021-00427-x.

[10] Z.M.S. Elbarbary, M.A. Alranini, Review of maximum power point tracking algorithms of PV system, Front. Eng. Built Environ. 1 (2021) 68–80, http://dx.doi.org/10.1108/febe-03-2021-0019.

[11] R.B. Bollipo, S. Mikkili, P.K. Bonthagorla, Hybrid, optimal, intelligent and classical PV MPPT techniques: A review, CSEE J. Power Energy Syst. 7 (2020) 9–33, http://dx.doi.org/10.17775/cseejpes.2019.02720.

[12] P. Kumari, N. Kumar, B.K. Panigrahi, A framework of reduced sensor rooftop SPV system using parabolic curve fitting MPPT technology for household consumers, IEEE Trans. Consum. Electron. 69 (2023) 29–37, http://dx.doi.org/10.1109/TCE.2022.3209974.

[13] S.R. Kiran, C.H. Basha, V.P. Singh, C. Dhanamjayulu, B.R. Prusty, B. Khan, Reduced simulative performance analysis of variable step size ANN based MPPT techniques for partially shaded solar PV systems, IEEE Access 10 (2022) 48875–48889, http://dx.doi.org/10.1109/access.2022.3172322.

[14] S. Echalih, A. Abouloifa, I. Lachkar, A.E. Aroudi, Z. Hekss, F. Giri, M.S. Al-Numay, A cascaded controller for a grid-tied photovoltaic system with three-phase half-bridge interleaved buck shunt active power filter: Hybrid control strategy and fuzzy logic approach, IEEE J. Emerg. Sel. Top. Circuits Syst. 12 (2022) 320–330, http://dx.doi.org/10.1109/JETCAS.2022.3152535.

[15] D.A. Nugraha, K.L. Lian, Suwarno, A novel MPPT method based on cuckoo search algorithm and golden section search algorithm for partially shaded PV system, Canadian J. Electr. Comp. Eng. 42 (2019) 173–182, http://dx.doi.org/10.1109/epec.2018.8598401.

[16] J.S. Koh, R.H.G. Tan, W.H. Lim, N.M.L. Tan, A modified particle swarm optimization for efficient maximum power point tracking under partial shading condition, IEEE Trans. Sustain. Energy 14 (2023) 1822–1834, http://dx.doi.org/10.1109/TSTE.2023.3250710.

[17] K. Sundareswaran, V. Vigneshkumar, P. Sankar, S.P. Simon, P.S.R. Nayak, S. Palani, Development of an improved P&O algorithm assisted through a colony of foraging ants for MPPT in PV system, IEEE Trans. Ind. Inform. 12 (2015) 187–200, http://dx.doi.org/10.1109/tii.2015.2502428.

[18] X. Zhang, S. Li, T. He, B. Yang, T. Yu, H. Li, L. Jiang, L. Sun, Memetic reinforcement learning based maximum power point tracking design for PV systems under partial shading condition, Energy 174 (2019) 1079–1090, http://dx.doi.org/10.1016/j.energy.2019.03.053.

[19] B. Yang, T. Yu, X. Zhang, H. Li, H. Shu, Y. Sang, L. Jiang, Dynamic leader based collective intelligence for maximum power point tracking of PV systems affected by partial shading condition, Energy Convers. Manage. 179 (2019) 286–303, http://dx.doi.org/10.1016/j.enconman.2018.10.074.

[20] B. Yang, L. Zhong, X. Zhang, H. Shu, T. Yu, H. Li, L. Jiang, L. Sun, Novel bio-inspired memetic salp swarm algorithm and application to mppt for PV systems considering partial shading condition, J. Clean. Prod. 215 (2019) 1203–1222, http://dx.doi.org/10.1016/j.jclepro.2019.01.150.

[21] S. Lyden, H. Galligan, M.E. Haque, A hybrid simulated annealing and perturb and observe maximum power point tracking method, IEEE Syst. J. 15 (2020) 4325–4333, http://dx.doi.org/10.1109/aupec.2015.7324803.

[22] S. Figueiredo, R.N.A.L. e Silva, Hybrid MPPT technique PSO-P&0 applied to photovoltaic systems under uniform and partial shading conditions, IEEE Lat. Am. Trans. 19 (2021) 1610–1617, http://dx.doi.org/10.1109/tla.2021.9477222.

[23] J. Ahmed, Z. Salam, An enhanced adaptive P&O MPPT for fast and efficient tracking under varying environmental conditions, IEEE Trans. Sustain. Energy 9 (2018) 1487–1496, http://dx.doi.org/10.1109/tste.2018.2791968.

[24] A. Gil-Velasco, C. Aguilar-Castillo, A modification of the perturb and observe method to improve the energy harvesting of PV systems under partial shading conditions, Energies 14 (2021) 2521, http://dx.doi.org/10.3390/en14092521.

[25] M.N. Ali, K. Mahmoud, M. Lehtonen, M.M. Darwish, An efficient fuzzy-logic based variable-step incremental conductance MPPT method for grid-connected PV systems, IEEE Access 9 (2021) 26420–26430, http://dx.doi.org/10.1109/access.2021.3058052.

[26] N. Kumar, I. Hussain, B. Singh, B.K. Panigrahi, Self-adaptive incremental conductance algorithm for swift and ripple-free maximum power harvesting from PV array, IEEE Trans. Ind. Inform. 14 (2017) 2031–2041, http://dx.doi.org/10.1109/tii.2017.2765083.

[27] S. Necaibia, M.S. Kelaiaia, H. Labar, A. Necaibia, E.D. Castronuovo, Enhanced auto-scaling incremental conductance MPPT method, implemented on low-cost microcontroller and SEPIC converter, Sol. Energy 180 (2019) 152–168, http://dx.doi.org/10.1016/j.solener.2019.01.028.

[28] H. Li, D. Yang, W. Su, J. Lü, X. Yu, An overall distribution particle swarm optimization MPPT algorithm for photovoltaic system under partial shading, IEEE Trans. Ind. Electron. 66 (2018) 265–275, http://dx.doi.org/10.1109/tie.2018.2829668.

[29] S. Obukhov, A. Ibrahim, A.A.Z. Diab, A.S. Al-Sumaiti, R. Aboelsaud, Optimal performance of dynamic particle swarm optimization based maximum power trackers for stand-alone PV system under partial shading conditions, IEEE Access 8 (2020) 20770–20785, http://dx.doi.org/10.1109/access.2020.2966430.

[30] K. Hu, S. Cao, W. Li, F. Zhu, An improved particle swarm optimization algorithm suitable for photovoltaic power tracking under partial shading conditions, IEEE Access 7 (2019) 143217–143232, http://dx.doi.org/10.1109/access.2019.2944964.

[31] W. Hayder, E. Ogliari, A. Dolara, A. Abid, B.H. M., L. Sbita, Improved PSO: a comparative study in MPPT algorithm for PV system control under partial shading conditions, Energies 13 (2020) 2035, http://dx.doi.org/10.3390/en13082035.

[32] S.K. Gopalakrishnan, S. Kinattingal, S.P. Simon, A.K. Kumar, Enhanced energy harvesting from shaded PV systems using an improved particle swarm optimisation, IET Renew. Power Gen. 14 (2020) 1471–1480, http://dx.doi.org/10.1049/iet-rpg.2019.0936.

[33] S. Obukhov, A. Ibrahim, A.A.Z. Diab, A.S. Al-Sumaiti, R. Aboelsaud, Optimal performance of dynamic particle swarm optimization based maximum power trackers for stand-alone PV system under partial shading conditions, IEEE Access 8 (2020) 20770–20785, http://dx.doi.org/10.1109/access.2020.2966430.

[34] S. Javed, K. Ishaque, S.A. Siddiqui, Z. Salam, A simple yet fully adaptive PSO algorithm for global peak tracking of photovoltaic array under partial shading conditions, IEEE Trans. Ind. Electron. 69 (2021) 5922–5930, http://dx.doi.org/10.1109/tie.2021.3091921.

[35] S. Javed, K. Ishaque, A comprehensive analyses with new findings of different PSO variants for MPPT problem under partial shading, Ain Shams Eng. J. 13 (2022) 1–14, http://dx.doi.org/10.1016/j.asej.2021.101680.

[36] S. Sharma, L. Varshney, R.M. Elavarasan, A.S.S. Vardhan, A.S.S. Vardhan, R. Saket, U. Subramaniam, E. Hossain, Performance enhancement of PV system configurations under partial shading conditions using MS method, IEEE Access 9 (2021) 56630–56644, http://dx.doi.org/10.1109/access.2021.3071340.

[37] V.B. Raju, C. Chengaiah, Performance analysis of conventional, hybrid and optimal PV Array configurations of partially shaded modules, Inter. J. Eng. Adv. Tech. 9 (2019) 3061–3073, http://dx.doi.org/10.35940/ijeat.a1661.109119.

[38] E.I. Batzelis, S.A. Papathanassiou, A method for the analytical extraction of the single-diode PV model parameters, IEEE Trans. Sustain. Energy 7 (2015) 504–512, http://dx.doi.org/10.1109/tste.2015.2503435.

[39] M. Hejri, H. Mokhtari, M.R. Azizian, M. Ghandhari, L. Söder, On the parameter extraction of a five-parameter double-diode model of photovoltaic cells and modules, IEEE J. Photovolt. 4 (2014) 915–923, http://dx.doi.org/10.1109/jphotov.2014.2307161.

[40] A. Ramadan, S. Kamel, M.M. Hussein, M.H. Hassan, A new application of chaos game optimization algorithm for parameters extraction of three diode photovoltaic model, IEEE Access 9 (2021) 51582–51594, http://dx.doi.org/10.1109/access.2021.3069939.

[41] S. Javed, K. Ishaque, A comprehensive analyses with new findings of different PSO variants for MPPT problem under partial shading, Ain Shams Eng. J. 13 (2022) 101680, http://dx.doi.org/10.1016/j.asej.2021.101680.

[42] A.P. Engelbrecht, Computational Intelligence: An Introduction, John Wiley & Sons, 2007.

[43] M. Jain, V. Saihjpal, N. Singh, S.B. Singh, An overview of variants and advancements of PSO algorithm, Appl. Sci. 12 (2022) 8392, http://dx.doi.org/10.3390/app12178392.

[44] S. Sharma, L. Varshney, R.M. Elavarasan, A.S.S. Vardhan, A.S.S. Vardhan, R. Saket, U. Subramaniam, E. Hossain, Performance enhancement of PV system configurations under partial shading conditions using MS method, IEEE Access 9 (2021) 56630–56644, http://dx.doi.org/10.1109/access.2021.3071340.

[45] P.K. Bonthagorla, S. Mikkili, Performance investigation of hybrid and conventional PV array configurations for grid-connected/standalone PV systems, CSEE J. Power Energy Syst. 8 (2020) 682–695, http://dx.doi.org/10.17775/cseejpes.2020.02510.